

ORIGINAL ARTICLE

Beyond 8% ultrathin kesterite $\text{Cu}_2\text{ZnSnS}_4$ solar cells by interface reaction route controlling and self-organized nanopattern at the back contact

Fangyang Liu^{1,4}, Jialiang Huang^{1,4}, Kaiwen Sun¹, Chang Yan¹, Yansong Shen², Jongsung Park¹, Aobo Pu¹, Fangzhou Zhou¹, Xu Liu¹, John A Stride³, Martin A Green¹ and Xiaojing Hao¹

Highly efficient, ultrathin (~400 nm) pure sulfide kesterite $\text{Cu}_2\text{ZnSnS}_4$ (CZTS) solar cells have been realized by interface reaction route controlling and self-organized nano-pattern at the back contact. The Al_2O_3 intermediate layer introduced at the Mo/CZTS interface can effectively inhibit the detrimental interfacial reaction between CZTS and Mo in the initial stage of sulfurization, and then turns into a self-organized nanopattern yielding a nanoscale opening for electrical contact. With this interface modification, the traditional issues of phase segregation (secondary phases) and voids at the back contact region can be well addressed, which greatly improves uniformity and reduces back contact recombination. As a result, this interface modification not only leads to beyond 8% ultrathin CZTS solar cells but also yields two certificated world record efficiencies: 9.26% for 0.237 cm^2 small area and 7.61% for 1 cm^2 standard kesterite CZTS solar cells (normal thickness).

NPG Asia Materials (2017) 9, e401; doi:10.1038/am.2017.103; published online 7 July 2017

INTRODUCTION

The semiconductor kesterite $\text{Cu}_2\text{ZnSnS}_4$ (CZTS) has attracted worldwide attention owing to its similarities with already commercialized direct gap absorbers such as CdTe and $\text{Cu}(\text{In,Ga})\text{Se}_2$ (CIGSe), while having only earth-abundant and environmentally friendly constituents. Good progress has been made over the past few years and the highest power conversion efficiency of 9.1% for sulfide CZTS¹ and 12.6% for sulfoselenide CZTS (CZTS(e))² solar cells have been achieved, demonstrating substantial commercial promise. Despite this progress in CZTS device, significant differences still exist when comparing CZTS with their Shockley–Queisser limit and CIGS devices. One of the most critical differences is the short minority carrier lifetime in CZTS of only several nanoseconds (ns), remarkably shorter than that of CIGSe (> 100 ns). Multiple reasons may contribute to the complexities of low CZTS lifetime, such as point defects, grain boundaries, intragrain crystallinity quality and secondary phases and so on.^{3–7} Despite the great efforts attempted to seek solutions to improve the lifetime such as defect engineering and passivation, an alternative solution would be to redesign an optimized device structure to accommodate present defective CZTS absorbers with short carrier lifetime. When designing a solar cell, a rough comparison between absorption length (L_a) and carrier diffusion length (L_d) and their relative sizes compared with the wavelength of visible light λ

determines how thick the absorber should be and the associated overall device design strategies. Current CZTS is a strong absorber ($L_a \approx \lambda$), while it has a moderate electronic quality ($L_d < \lambda$). For a semiconductor absorber with short lifetime, which is indicative of a short diffusion length, efficient current extraction is possible only when the distance that minority carriers need to travel is reduced. This can be realized by intentionally making the active absorber thinner. In addition, thinning the absorber is also favorable to enhance manufacturing throughput and reduce the material usage. However, this would result in two problems: First, reducing the absorber thickness leads to incomplete absorption of incident photons. According to previous experience in ultrathin CIGSe solar cells, this issue of optical losses can be minimized by improved back contact reflectivity^{8,9} and implementation of light trapping,^{10–12} both of which could be well used in the case of ultrathin CZTS. Second, thinning the absorber makes recombination of minority electrons at the back contact more obvious and quality control more challenging.¹³ For ultrathin CIGSe solar cells, the recombination at back contact region could be reduced by introducing back-surface field via $[\text{Ga}]/([\text{Ga}]+[\text{In}])$ grading^{14,15} and rear surface passivation.^{8,16} However, for ultrathin CZTS(e) solar cells, the quality of CZTS(e) and associated back contact recombination issues are much more serious. This is because the CZTS(e)/Mo interface is not as chemically

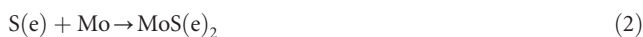
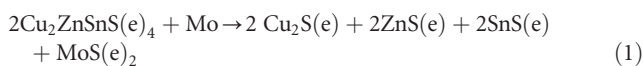
¹School of Photovoltaic and Renewable Energy Engineering, TETB248, School of Photovoltaic and Renewable Energy Engineering, University of New South Wales, Sydney, NSW, Australia; ²School of Chemical Engineering, University of New South Wales, Sydney, NSW, Australia and ³School of Chemistry, University of New South Wales, Sydney, NSW, Australia

⁴These authors contributed equally to this work.

Correspondence: Dr X Hao, School of Photovoltaic and Renewable Energy Engineering, TETB248, School of Photovoltaic and Renewable Energy Engineering, University of New South Wales, High Street Kensington, Sydney, NSW 2052, Australia.
E-mail: xj.hao@unsw.edu.au

Received 22 February 2017; revised 2 April 2017; accepted 2 April 2017

stable as that of CIGSe/Mo interface. The Mo back contact is relatively inert with CIGSe, but reacts with CZTS(e) (see reaction (1)), which is energetically favorable according to thermodynamic calculations.¹⁷ This reaction leads to the decomposition of CZTS(e) into secondary phases, that is, ZnS(e), SnS(e) and Cu_{2-x}S(e), and the formation of a thick MoS(e)₂ interfacial layer. The segregation of secondary phases reduces the quality and uniformity of CZTS(e) absorber, enhancing the recombination. Moreover, the escape of SnS(e) phase owing to its high volatility¹⁸ and the migration of Cu into the absorber and MoS(e)₂^{19–22} owing to its high diffusivity usually leave voids and ZnS(e) behind at the CZTS/Mo interfacial region.^{23,24} Both voids and ZnS(e) reduce the effective volume of the absorber, which may have limited impact on normal absorber thickness (over 800 nm), but is unfavorable for ultrathin CZTS(e) solar cells. In addition, the phase segregation-induced defects¹⁷ may enhance the recombination at the back contact and voids may result in shunt problems, which both would be more pronounced in ultrathin solar cells. MoS(e)₂ is formed through interfacial reactions (1) and/or (2), depending on the process conditions, and it is the MoS(e)₂ that is the ‘real’ part of back contact directly connecting to kesterite. Similar to the case of CIGSe solar cells,²⁵ on the one hand, the MoS(e)₂ is beneficial and necessary for providing a high work function, electrical quasi-ohmic contact and good adhesion for CZTS(e).²¹ On the other hand, if the MoS(e)₂ is too thick, this leads to high series resistance and accordingly deteriorates the device efficiency.²⁶ To eliminate the chemical incompatibility between CZTS(e) and Mo, alternative back contacts or interface deactivation using barrier layers are possible. Altamura *et al.*²⁷ have reported that W and Au are eligible alternative back contacts because of their higher J_{sc} compared to Mo, but Mo remains the best back contact in terms of energy conversion efficiency.²⁷ Interface deactivation using a barrier layer has been studied intensively in the past several years, such as ZnO,^{28,29} TiN,^{30,31} TiB₂,²¹ Ag³² and C.²³ It is still very challenging to avoid the void and secondary phase issues whilst maintaining the advantages of Mo contact



In this communication, we report ultrathin (~400 nm) Se-free kesterite CZTS solar cells of > 8% efficiency, realized by inserting an ultrathin dielectric intermediate layer (sputtered Al₂O₃ is chosen here, but other stable dielectric materials such as SiO₂ or ZrO₂, etc. may also be applicable) into the Mo/CZTS interface. This dielectric Al₂O₃ intermediate layer, obtained from low-cost and high-throughput sputtering methods, initially prevents the direct contact of CZTS with Mo, and thereby suppresses the decomposition of CZTS by the chemical reaction (1). The desired thin MoS₂ layer can be formed by reacting Mo with sulfur diffused from a sulfur-contained atmosphere during sulfurization process for fabricating CZTS absorber according to reaction (2). The initially continuous Al₂O₃ layer then transforms to a nanopatterned surface with microstructure change during the formation of MoS₂. This self-organized Al₂O₃ nano-pattern makes openings for the direct connection of CZTS with MoS₂, thereby maintaining the advantages of the Mo back contact material. Therefore, the purpose and mechanisms of this inserted Al₂O₃ layer is totally different from that deposited on the front surface of absorber for defect passivation and on buffer for avoiding damage from transparent conductive oxide sputtering.³³ By controlling the interfacial reaction via this intermediate layer, the highest 8.5% efficient ultrathin kesterite CZTS thin film solar cell is achieved

without notable phase segregation and voids and with reduced recombination at the back contact region. It is notable that this is the first report of efficiencies beyond 8% in ultrathin CZTS solar cells realized through a simple self-organized nanopattern and well-improved CZTS film quality, which demonstrates great promise though lower than the present highest 12.3% efficient ultrathin CIGSe solar cells with more complicated scattering dielectric scattering patterns.¹⁰

EXPERIMENTAL PROCEDURES

Ultrathin CZTS solar cell configuration of Mo/CZTS/buffer/ intrinsic ZnO/indium tin oxide /Al was used in this study. CZTS absorbers with a thickness of only 400 nm were prepared by sulfurization of cosputtered Cu/ZnS/SnS precursors by a magnetron sputtering system (AJA International (Scituate, MA, USA); model ATC-2200) on Mo-coated soda lime glass substrates. CZTS absorbers with normal thickness of ~800 nm were also fabricated for comparison. The sulfurization process was performed in a combined sulfur and SnS atmosphere at 560 °C with a heating rate of 15 °C min⁻¹ for 5 min. The average composition of the CZTS absorbers is controlled to be Cu-poor and Zn-rich (atomic ratio Cu/Sn=1.80 and Zn/Sn=1.15 measured by energy dispersive X-ray spectroscopy). Buffer layers of CdS with a thickness of 50 nm were prepared by chemical bath deposition method. Specifically, cadmium sulfate (3CdSO₄·8H₂O), excess thiourea (H₂NCSNH₂) and ammonium hydroxide were mixed with a base environment for CdS deposition, with details shown elsewhere.³⁴ The 50 nm intrinsic ZnO and 300 nm indium tin oxide films were deposited by radio frequency sputtering. Al grids by evaporation were used as the top contact. The final step in the device fabrication sequence is the deposition of an antireflection coating (110 nm MgF₂). The total area of the final cells is 0.45 cm², defined by mechanical scribing.

The microstructure and elemental distribution across the CZTS and buffer interface were measured by JEOL JEM-ARM200F (200 kV) aberration-corrected scanning transmission electron microscope (Peabody, MA, USA) equipped with energy-dispersive X-ray spectroscopy system. The ESCALAB250Xi (Thermo Scientific, Loughborough, UK) was used to conduct X-ray photoelectron spectroscopy measurements in which the X-ray source was monochromated Al K α (1486.68 eV). Na depth profiling data were achieved by sputtering the surfaces of CZTS with 3 keV Ar⁺ ions with reference etching rate of 0.36 nm s⁻¹ for Ta₂O₅ over an etching area of 2.5 × 2.5 mm². Before measurement, the surface was cleaned 30 s by 3 keV Ar⁺ ions etching to remove possible surface contamination. The Raman measurements were carried out by Jobin-Yvon LabRAM HR-800 (Kyoto, Japan) with a laser wavelength of 514 nm and 325 nm at room temperature. Time-resolved photoluminescence (TRPL) measurements were performed on devices using the time-correlated single photon counting technique (Microtime200, Picoquant) at a wavelength of 800 nm at room temperature. The excitation source is a 640 nm laser, which can penetrate through the window layers (intrinsic ZnO and indium tin oxide) and buffer layer CdS, and reach deeper position, close to the bottom of the ultrathin CZTS absorber, than 457 nm laser used in the previous CZTS/buffer interface investigations.³⁵ In-house current density–voltage (J–V) characterizations of CZTS devices were performed using a solar simulator (Newport, Irvine, CA, USA) with a AM1.5 illumination and an intensity of 100 mW cm⁻² calibrated with a standard Si reference cell traceable to the Fraunhofer Institut für Solare Energiesysteme. External quantum efficiency data were collected by a QEX10 spectral response system (PV Measurements, Point Roberts, WA, USA) calibrated by the National Institute of Standards and Technology-certified reference Si photodiode. This system uses monochromatic light chopped at a frequency of 120 Hz. The 7.61% efficiency for 1 cm² device (1.067 cm²) and 9.26% efficiency for small area device (0.237 cm²) were independently certified by the National Renewable Energy Laboratory (Golden, CO, USA) and Newport Corporation (Irvine, CA, USA), respectively. The certified device power conversion efficiency is consistent (within 1%, absolute) with the value measured in-house.

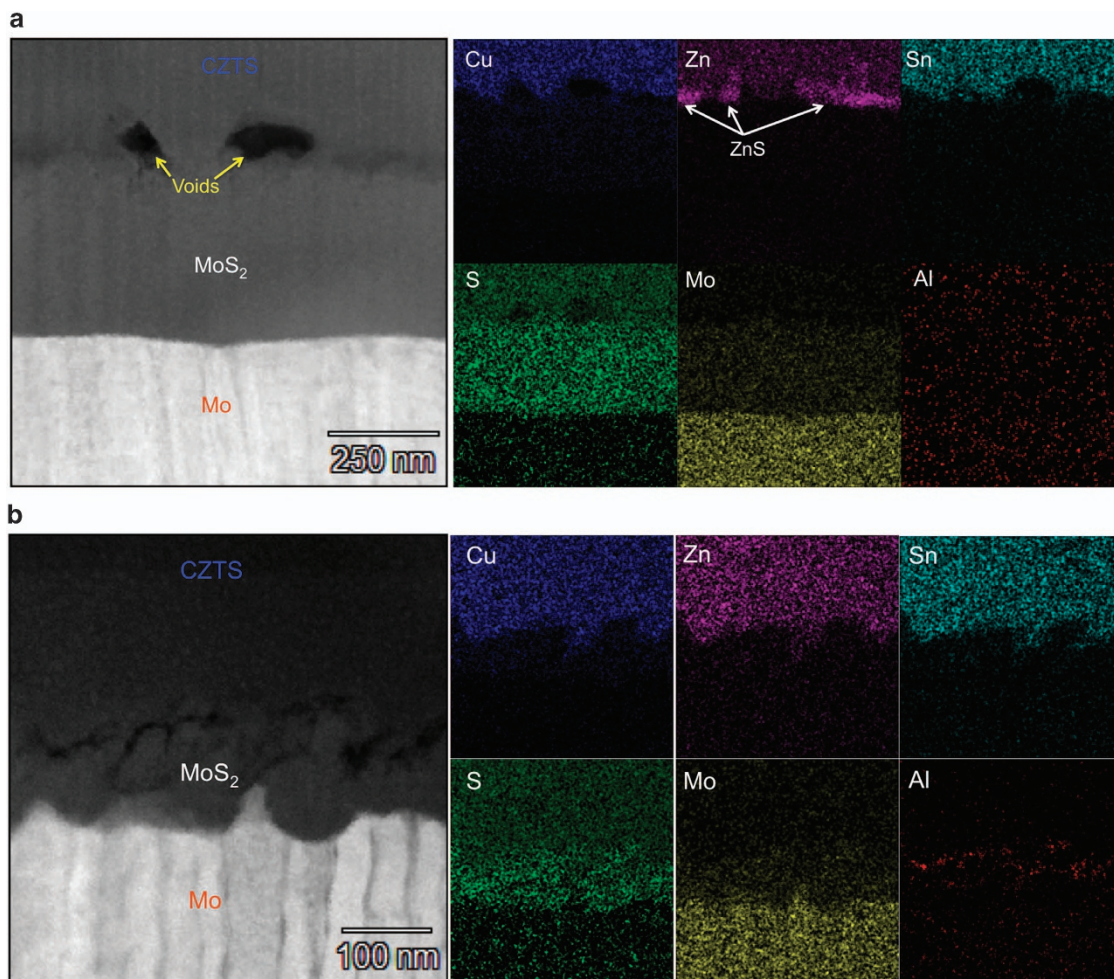


Figure 1 Cross-sectional transmission electron microscope (TEM) images and energy-dispersive X-ray spectroscopy (EDS) mapping for back-contact regions of ultrathin Cu₂ZnSnS₄ (CZTS) devices without (a) and with (b) Al₂O₃ intermediate layer.

RESULTS AND DISCUSSION

The microstructure of ultrathin CZTS with and without Al₂O₃ layer demonstrates a significant difference. Figure 1a shows the typical transmission electron microscopy (TEM) cross-sectional image (high-angle annular dark field) and energy-dispersive X-ray spectroscopy (EDS) elemental mapping taken from the interfacial region at the back contact of a typical ultrathin CZTS solar cell without any intermediate layer. From the TEM cross-sectional image, voids at the back contact can be clearly observed and the thickness of the MoS₂ interfacial layer is as high as 300 nm. From the EDS elemental composition maps, bright domains in the composition map of Zn are detected at the bottom of the CZTS, indicating lumps of ZnS. The slight difference in the brightness of Cu and Sn at the corresponding location suggests the existence of Zn-based secondary phase only, that is, ZnS segregation at the back contact region. After inserting a thin Al₂O₃ intermediate layer (about 3 nm) into the CZTS and Mo interface, as shown in Figure 1b, the voids and ZnS segregation are absent and the MoS₂ interfacial layer shows the thickness of only ~100 nm. By careful comparison, some black contrasts, which are not continuous and result from element(s) with lower atomic number for high-angle annular dark field,³⁶ can be observed between the CZTS and MoS₂. Combining the composition map of Al, these black contrasts correspond to the dispersed Al₂O₃ aggregates. This indicates that the introduced Al₂O₃ intermediate layer sputtered on the Mo

back contact turns into discontinuous aggregates after sulfurization, which could form nanopatterned Al₂O₃ arrays between CZTS and MoS₂ with openings for their connection.

High-resolution TEM images of the interface region at the back contact provides more details about microstructure evolution and interfacial reactions. As shown in Figure 2, before sulfurization of the CZTS precursor, the ultrathin (1–5 nm) Al₂O₃ intermediate layer deposited by radio frequency sputtering, is continuous and covers the Mo substrate very well (see Figure 2a), which can be further confirmed by low magnification TEM image in Supplementary Figure S1. Therefore, the direct contact of the CZTS precursor and Mo, which is the typical configuration in the conventional fabrication process, can be prevented. Upon sulfurization, in the initial stage, reaction (1) between CZTS and Mo can be effectively avoided. MoS₂ in this case can only be generated through reaction (2), where Mo reacts with S from the sulfur-contained sulfurization atmosphere diffusing through CZTS²⁶ and Al₂O₃. The formation of MoS₂ is accompanied by a marked change in the surface microstructure, which can be evidenced by the atomic force microscopy images in Supplementary Figure S2 taken from sulfurized bare or 3 nm Al₂O₃-coated Mo-SLG substrates. This leads to the breaking of the Al₂O₃ layer into discontinuous aggregates, as seen in Figure 2b, producing a self-organized Al₂O₃ nanopattern. The openings between Al₂O₃ aggregates facilitate the direct connection of CZTS and MoS₂ for electrical contact and

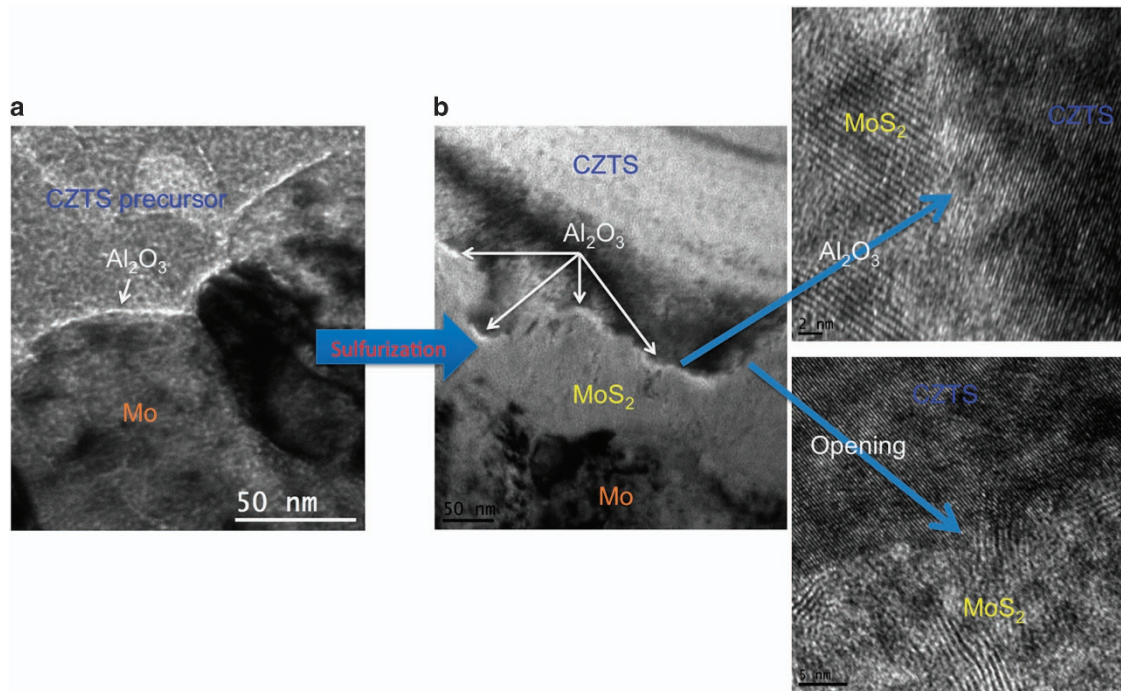


Figure 2 High-resolution transmission electron microscope (HRTEM) images of back contact regions showing the microstructure evolution during sulfurization (a) before sulfurization, (b) after sulfurization.

good adhesion, and the initially formed MoS_2 at the opening region then acts as a barrier to further avoid the direct contact of CZTS and Mo. Therefore, in the whole sulfurization process, reaction (1) can be prevented and the formation of MoS_2 can only proceed via reaction (2). In this situation, the voids and ZnS segregation at the back contact region resulting from reaction (1) are well avoided, and the thickness of the MoS_2 layer can be controlled at ~ 100 nm. Moreover, the advantages of a Mo back contact could be retained via the direct connection of CZTS and MoS_2 at the openings. The short distance of only several tens of nanometers between openings is beneficial to shorten the majority-carriers' transmission path and avoid high series resistance (R_s) of the final device. In this case, current can flow through these opening regions easily, and the other regions of the CZTS contacting with Al_2O_3 aggregates may be passivated according to previous reports on both CZTS³⁷ and CIGSe.^{16,38} It is notable that these previous papers^{16,36,37} reported several tens of nanometers Al_2O_3 used for defect passivation based on the reasoning of back surface field effect from its negative charges, which is well known in the Si solar cell technology. In their case, openings are usually specially designed and fabricated for obtaining electrical contact, making the cell fabrication process more complex, challenging and difficult for upscaling. In contrast, in this work, the ultrathin (only a few nanometer) dielectric Al_2O_3 (SiO_2 and ZrO_2 , etc. may also work) intermediate layer into the Mo/CZTS interface is developed for controlling/designing the CZTS/Mo back contact chemical reaction route. That is to say, the ultrathin dielectric layer allows limited thickness (within 100 nm) of MoS_2 to form at the initial stage of sulfurization, and then dielectric layer turns into self-organized nanopattern with nanoscale opening for current transport.

Although the introduction of the Al_2O_3 intermediate layer could control the back contact interface reaction occurring only by reaction (2), its effects on the properties of CZTS absorbers still need to be evaluated. By comparing the scanning electron microscopy

(magnification $\times 80\,000$) surface morphology of the CZTS absorbers without (Figure 3a) and with (Figure 3b) Al_2O_3 intermediate layer at back contact (lower magnification $\times 20\,000$ scanning electron microscopy morphology is also shown in Supplementary Figure S3), it can be observed that the absorber with Al_2O_3 intermediate layer shows more compact morphology without pin holes. Both CZTS absorbers consist of well-crystallized grains and some of the grains show a size larger than $1\ \mu\text{m}$. However, it is notable that the CZTS absorber without an Al_2O_3 intermediate layer at the back contact shows a less uniform grain size distribution with smaller grains. Better homogeneity and compactness for the CZTS absorber with an Al_2O_3 intermediate layer at the back side can be observed from the comparison of the low-magnification TEM cross-sectional images in Supplementary Figures S4a and b, in addition to much thinner MoS_2 interface layer and less consumption of Mo, which is favorable to low series resistance. It should be pointed out that some white/bright dots that segregate out can be observed on CZTS absorber with Al_2O_3 intermediate layer at back contact. From the Raman spectra recorded using an excitation wavelength of 325 nm, as shown in Supplementary Figure S5, three peaks arising from the first-, second- and third-order ZnS bands show much higher intensity, indicating much more ZnS at the surface region for CZTS absorber with Al_2O_3 intermediate layer at back contact. Therefore, these dots can be reasonably assigned to precipitated ZnS, which appears white/bright because of the charging effect of a less conductive phase.³⁹ It is notable that these ZnS dots may not have significant negative effect on device performance, except reducing the effective volume of the absorber.²⁰ It also should be mentioned that, for CZTS absorber without Al_2O_3 intermediate layer at back contact, the detectable ZnS (although very little) by Raman measurement using 325 nm excitation seems to be mostly located around the pin holes from the distribution of the white/bright features. This implies that the formation of pin hole might be related to the decomposition of CZTS. The elimination of pin holes by

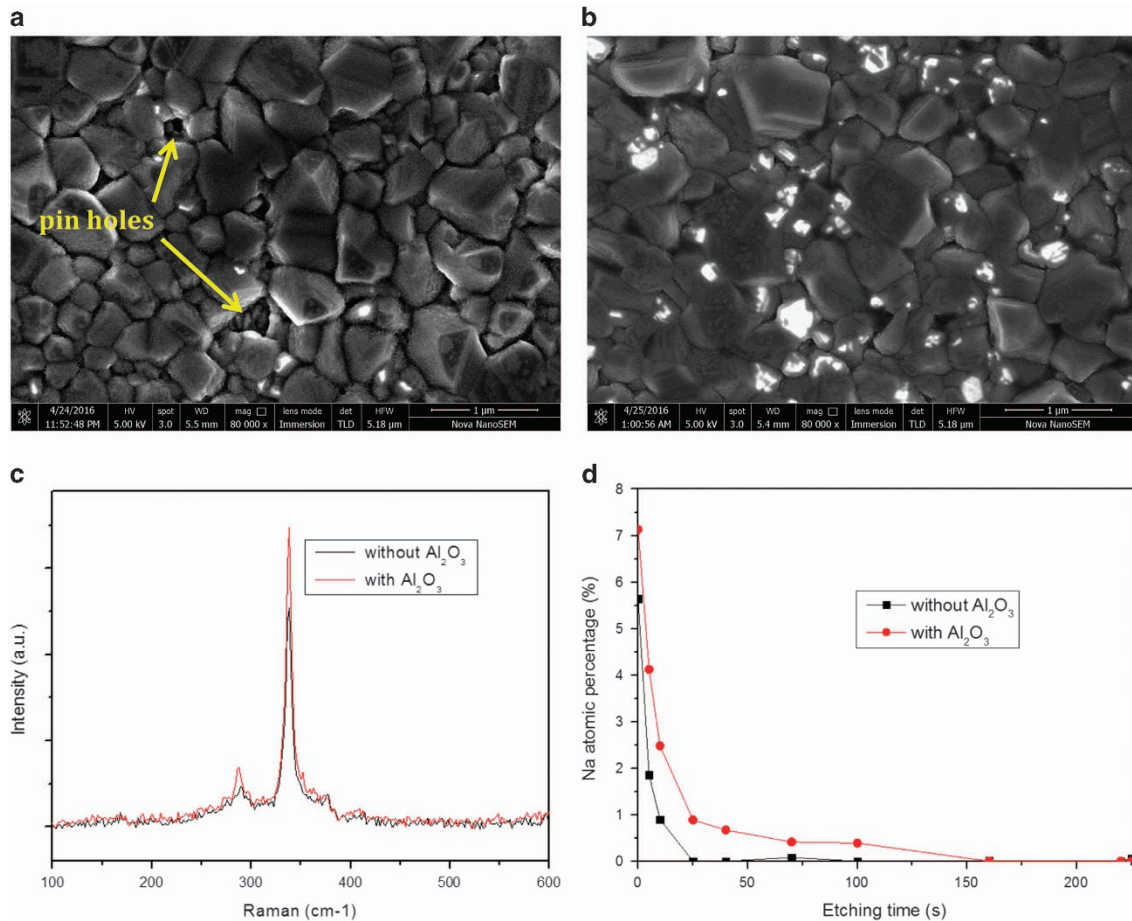


Figure 3 Scanning electron microscopy (SEM) morphologies of ultrathin CZTS absorbers on Mo without (a) and with (b) Al₂O₃ intermediate layer; Raman spectra from 514 nm excitation (c) and Na profiles by X-ray photoelectron spectroscopy (XPS) (d) of Cu₂ZnSnS₄ (CZTS) absorbers on Mo with and without Al₂O₃ intermediate layer.

Al₂O₃ intermediate layer suggests the inhibited decomposition of CZTS (via interface reaction (1) most likely). Comparison of Raman spectra by 514 nm excitation (the depth of the measurement is ~ 100 nm; Ito⁴⁰), Figure 3c indicates that, after inserting the Al₂O₃ intermediate layer, the phase purity that is retained (in the range of the Raman measurement), and the main characteristic peak of CZTS (338 cm^{-1}) shows higher intensity and smaller full-width at half-maximum value (from $3.95 \pm 0.02\text{ cm}^{-1}$ it decreased to $3.55 \pm 0.02\text{ cm}^{-1}$), suggesting a relatively better crystalline quality. In our previous report²¹ on back contact modification by TiB₂ intermediate layer from 10 to 70 nm, the crystallinity of the CZTS became worse, leading to the degradation in V_{oc} of the final device, which is most likely due to the inhibition of Na diffusion by the thick and continuous intermediate layer. In this work, from the Na distribution profiles measured by X-ray photoelectron spectroscopy (detection limit $\sim 0.1\text{at}\%$) in Figure 3d, one can observe that Na accumulates at the upper part for both absorbers, and the absorber with Al₂O₃ intermediate layer at the back side shows a higher Na content. Considering that impact of environment on Na distribution is slight⁴¹ and should be the same on both CZTS absorbers with or without Al₂O₃ intermediate layer at back contact, it is believed that the difference in Na profile should be from the Al₂O₃ modification at back contact. Therefore, the difference in Na profiles should be related to the voids-free microstructure of the interface at the back contact in the case of the Al₂O₃ intermediate layer. This is because the voids can

act as a space barrier, blocking Na diffusion from soda-lime glass into the CZTS absorber. In addition, this blocking of Na diffusion by voids may lead to a nonuniform Na diffusion and distribution in the absorber, which might be responsible for the nonuniform grain size in aforementioned scanning electron microscopy observation.

Besides, from the EDS line scan in Supplementary Figure S6, crossing from absorber to Mo, the out-diffusion of Cu into MoS₂ interfacial layer still can be observed, similar to the conventional configuration.^{2,19–22} The role of this Cu out-diffusion is unknown, but the incorporation of Cu into MoS₂ may be helpful in reducing the resistivity of MoS₂,⁴² and the interaction between absorber and back contact via Cu may improve the adhesion according to the previous experience in the CIGS case.⁴³

Figure 4a shows the J–V curves of the best ultrathin CZTS solar cells with and without Al₂O₃ intermediate layer at back contact. The performance parameters deduced from J–V measurements are summarized in Table 1, and the box-plot diagram of statistical data is shown in Supplementary Figure S7 to make the comparison reliable. We can observe substantial enhancement in open circuit voltage (V_{oc}) and fill factor (FF), as well as a slight increase in the short circuit current (J_{sc}) for the device with an Al₂O₃ intermediate layer at the back contact. Correspondingly, the conversion efficiency is significantly boosted from 7.34 to 8.57%. The enhancement in V_{oc} and FF, accompanied by an increase in R_{sh} and reduction in the ideality factor (A) and reverse saturation current (J_0), is a clear

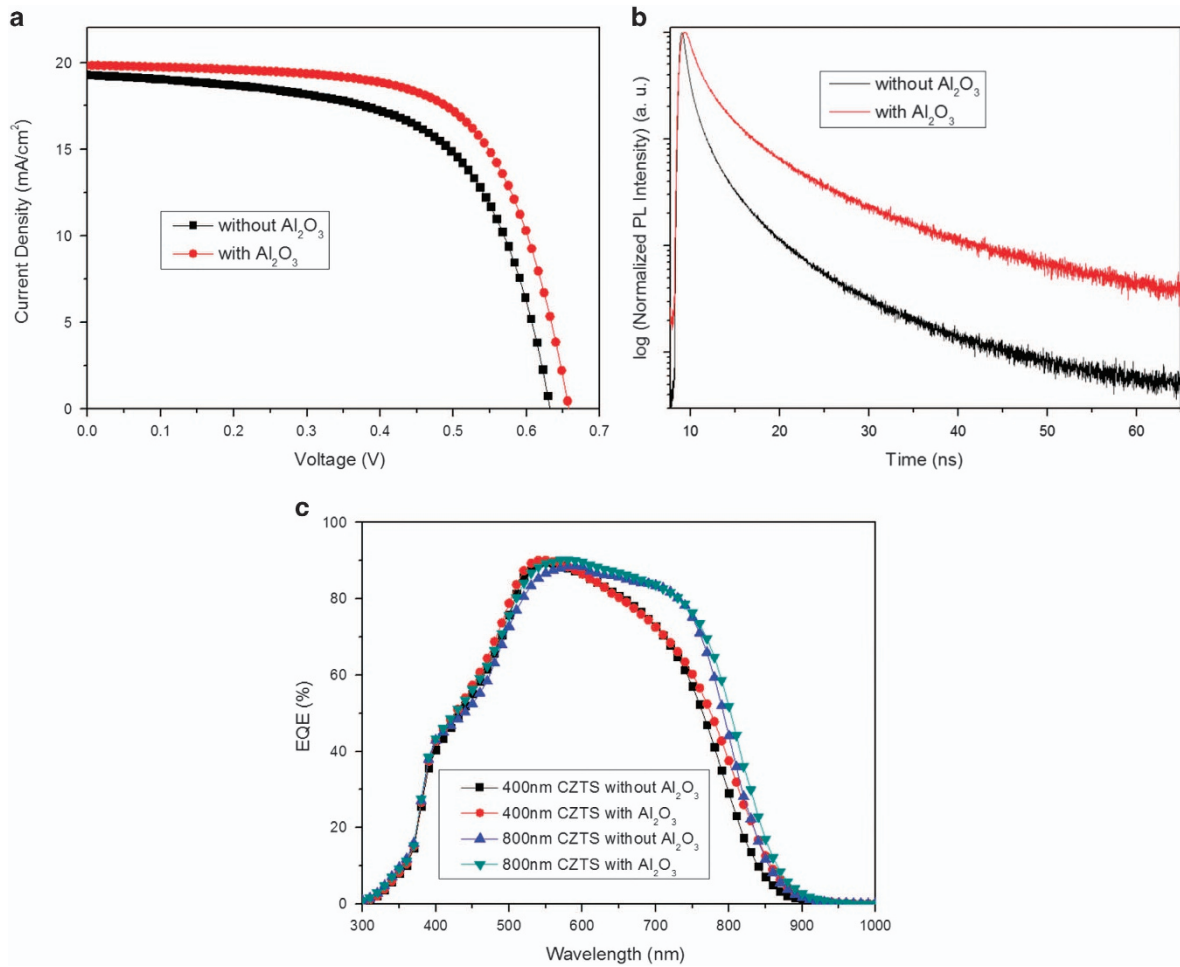


Figure 4 (a) Current density–voltage (J – V), (b) time-resolved photoluminescence and (c) external quantum efficiency (EQE, 0 bias) curves for ultrathin $\text{Cu}_2\text{ZnSnS}_4$ (CZTS) devices (0.45 cm^2) with and without Al_2O_3 intermediate layer.

Table 1 Device characteristics of the ultrathin CZTS solar cells (0.45 cm^2) with various processes

$\text{Al}_2\text{O}_3(\text{nm})$	$V_{oc} (\text{mV})$	$J_{sc} (\text{mA cm}^{-2})$	FF (%)	Efficiency (%)	$R_{s,L}(\Omega \text{ cm}^2)$	$R_{sh,L}(\Omega \text{ cm}^2)$	A	$J_0(\text{mA cm}^{-1})$
0	632.0	19.00	61.12	7.34	1.60	444.70	1.65	6.33×10^{-6}
3	657.8	19.76	65.91	8.57	1.97	1424.05	1.57	3.10×10^{-6}

Abbreviations: CZTS, $\text{Cu}_2\text{ZnSnS}_4$; FF, fill factor; J_{sc} , short circuit current; V_{oc} , open circuit voltage.

To make data comparable with other groups such as IBM,² the series resistance under light ($R_{s,L}$), ideality factor A and reverse saturation current (J_0) are determined from light J – V data using the Sites' method.⁴⁶

indication of the reduced recombination from the eliminated phase segregation and voids at the back contact region, coupled with the pin-hole-free morphology and improved crystalline quality (bulk recombination). The TRPL measurements were performed on CZTS devices as shown in Figure 4b to check the minority carrier lifetime. Before TRPL measurements, PL spectra were also recorded as shown in Supplementary Figure S8, demonstrating the weaker PL intensity for the device without Al_2O_3 intermediate layer at the back contact. The lifetime is estimated from the TRPL traces, according to a previously reported method,⁴⁴ to be 10.1 and 7.6 ns, respectively, for CZTS with and without the Al_2O_3 intermediate layer. This indicates that inserting the Al_2O_3 intermediate layer at the back contact can effectively passivate defects and improve the lifetime, in other words reduce recombination, which partially accounts for the higher V_{oc} and FF of the final device. The slight increase in J_{sc} from

the better collection in the long wavelength region, as shown in Figure 4c, can be related to better crystalline quality, longer minority carrier lifetime and decreased MoS_2 thickness, which also contribute to FF improvement. However, the J_{sc} is still lower than the devices using absorber with a normal thickness (800 nm) as seen in Supplementary Figure S9 and Supplementary Table S1. From the external quantum efficiency comparison in Figure 4c, it is indicative that the main loss for ultrathin CZTS devices is in the long wavelength region, suggesting insufficient absorption of incident long wavelength photons. The enhancement in optical absorption by back contact configuration optimization is under investigation (not the focus of this work) and will be reported elsewhere.

The introduction of the Al_2O_3 intermediate layer at the back contact to control the interface reaction and improve the performance of ultrathin CZTS devices is also applicable in normal CZTS devices.

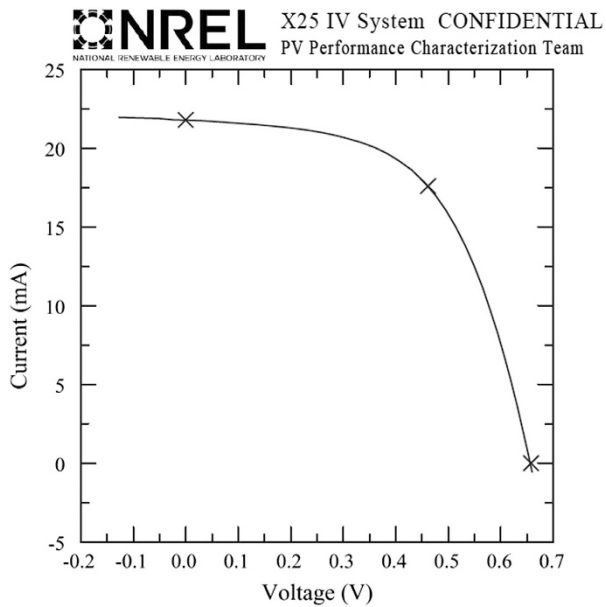


Figure 5 Current–voltage curve of 1.067 cm² normal Cu₂ZnSnS₄ (CZTS) device (800 nm CZTS absorber) with 7.61% efficiency independently tested by National Renewable Energy Laboratory (NREL).

Supplementary Figures S10 and S11 show the TEM cross-sectional image and EDS elemental mapping images taken from the interfacial region at the back contact of CZTS devices using an absorber of the normal thickness of 800 nm. Compared with the ultrathin case without an Al₂O₃ intermediate layer at the back contact, the voids and ZnS phase segregation appear more pronounced. This may be due to the limited sulfur diffusion through CZTS, thereby inhibiting or suppressing reaction (2) in the initial stage of sulfurization, as according to the kinetics analysis of the formation of the MoSe₂ interface layer by reaction (2), it is limited by the diffusion of Se through the CZTSe layer.²⁶ The voids and ZnS phase segregation can be eliminated by introducing an Al₂O₃ intermediate layer at the back contact, showing the same behavior as ultrathin CZTS cases. The conversion efficiency of the normal CZTS device is comparable to that of an ultrathin CZTS device; however, by comparing the electrical parameters, one can find that the normal CZTS device shows a higher J_{sc} because of a greater optical absorption, but lower V_{oc} and FF, which indicates a problem of bulk recombination. The efficiency of the normal CZTS device can be enhanced with the introduction of an Al₂O₃ intermediate layer at the back contact from 7.50 to 8.27%, with an improvement in all parameters including V_{oc} , J_{sc} and FF, as shown in Supplementary Figure S9. Considering that the Al₂O₃ intermediate layer improves the homogeneity and compactness of the CZTS absorber, we have also fabricated 1 cm² standard CZTS device. The current–voltage curve independently tested at the National Renewable Energy Laboratory is shown in Figure 5 (more test details can be seen in Supplementary Figure S12), indicating 7.61% efficiency (size of 1.067 cm²) with V_{oc} of 657.9 mV, J_{sc} of 20.41 mA cm⁻² and FF of 56.65%. This is the world record efficiency for 1 cm² sulfide kesterite CZTS solar cells. Nevertheless, because the performance of the normal CZTS device is still low, especially in FF (as well as V_{oc}), further optimization on absorber process to reduce bulk recombination is obviously very necessary. Up to now, the best performance of the normal CZTS device with Al₂O₃ intermediate layer at the back contact and further optimized absorber process has achieved efficiency of 9.26% (cell area of 0.237 cm²) with V_{oc} of 662 mV,

J_{sc} of 20.72 mA cm⁻² and FF of 67.5%, independently certified by Newport Corporation as seen in Supplementary Figure S13. This is also the new world record efficiency (regardless of cell area) for sulfide kesterite CZTS solar cells.

The effects of the thickness of the Al₂O₃ intermediate layer were also investigated. It was found that no obvious effects on device performance could be observed when the thickness was only 1 nm owing to the fact that the Al₂O₃ layer, deposited by sputtering, is not continuous at such a thickness, while at a thickness of > 5 nm led to serious delamination of the CZTS absorbers. The thickness of 2–3 nm has been found to be most suitable in our experimental system. Atomic layer deposition may provide a possible route to deposit continuous Al₂O₃ film at thicknesses lower than 1 nm,⁴⁶ and can be considered in future process optimization. Besides, Al₂O₃ might be replaced by other similar dielectric materials such as SiO₂¹⁰ or ZrO₂ and so on, which is under investigation. It also should be remarked that the insight from this interface modification at back contact has the potential to be of importance for designing/fabricating other solar cells such as Cu(In,Ga)Se₂, or electronic devices, which need to structure a large area electrical contact and/or have similar interface problems.

CONCLUSION

In summary, we have shown an effective way to control interfacial reactions at the back contact in fabricating efficient ultrathin CZTS solar cells. By introducing an Al₂O₃ intermediate layer between Mo and CZTS, the voids and phase segregation at the back contact region can be well eliminated by inhibiting the interface reaction between CZTS and Mo at the initial stage of sulfurization. After sulfurization, the Al₂O₃ intermediate layer will be transformed to self-organized nanopattern, with selective openings for electrical contact enabling current transport. The quality of CZTS also becomes better, showing longer minority lifetime. With the Al₂O₃ intermediate layer, the conversion efficiency of the ultrathin CZTS solar cells can be improved from 7.34 to 8.56%. This interface modification has been proved effective and reproducible in normal thickness CZTS devices, which yields our recent two world record efficiencies: 7.61% for 1 cm² standard (1.067 cm²) and 9.26% for small area (0.237 cm²) CZTS solar cells. The future work will be mainly focused on enhancing optical absorption and thereby short circuit current as well as further improvements in the interface and absorber quality.

CONFLICT OF INTEREST

The authors declare no conflict of interest.

ACKNOWLEDGEMENTS

This Program has been supported by the Australian Government through the Australian Renewable Energy Agency (ARENA, 1-USO028) and Australian Research Council (ARC, LP110200651) and Guodian New Energy Technology Research Institute. Responsibility for the views, information or advice expressed herein is not accepted by the Australian Government. We also thank Dr Xiaoming Wen at the University of New South Wales for TRPL measurements, and David Mitchell at the University of Wollongong for TEM and energy dispersive X-ray spectroscopy tests.

- 1 Green, M. A., Emery, K., Hishikawa, Y., Warta, W. & Dunlop, E. D. Solar cell efficiency tables (version 46). *Prog. Photovolt.* **23**, 805–812 (2015).
- 2 Wang, W., Winkler, M. T., Gunawan, O., Gokmen, T., Todorov, T. K., Zhu, Y. & Mitzi, D. B. Device characteristics of CZTSe thin-film solar cells with 12.6% efficiency. *Adv. Energy Mater.* **4**, 1301465 (2014).

- 3 Zhou, H., Song, T.-B., Hsu, W.-C., Luo, S., Ye, S., Duan, H.-S., Hsu, C.-J., Yang, W. & Yang, Y. Rational defect passivation of Cu₂ZnSn(S,Se)₄ photovoltaics with solution-processed Cu₂ZnSnS₄:Na nanocrystals. *J. Am. Chem. Soc.* **135**, 15998–16001 (2013).
- 4 Werner, M., Keller, D., Haass, S. G., Gretener, C., Bissig, B., Fuchs, P., La Mattina, F., Erni, R., Romanyuk, Y. E. & Tiwari, A. N. Enhanced carrier collection from CdS passivated grains in solution-processed Cu₂ZnSn(S,Se)₄ solar cells. *ACS Appl. Mater. Inter.* **7**, 12141–12146 (2015).
- 5 Walsh, A., Chen, S. Y., Wei, S. H. & Gong, X. G. Kesterite thin-film solar cells: advances in materials modelling of Cu₂ZnSnS₄. *Adv. Energy Mater.* **2**, 400–409 (2012).
- 6 Li, J. B., Chawla, V. & Clemens, B. M. Investigating the role of grain boundaries in CZTS and CZTSSe thin film solar cells with scanning probe microscopy. *Adv. Mater.* **24**, 720–723 (2012).
- 7 Romero, M. J., Du, H., Teeter, G., Yan, Y. & Al-Jassim, M. M. Comparative study of the luminescence and intrinsic point defects in the kesterite Cu₂ZnSnS₄ and chalcopyrite Cu(In,Ga)Se₂ thin films used in photovoltaic applications. *Phys. Rev. B* **84**, 165324 (2011).
- 8 Vermang, B., Wätjen, J. T., Fjällström, V., Rostvall, F., Edoff, M., Kotipalli, R., Henry, F. & Flandre, D. Employing Si solar cell technology to increase efficiency of ultra-thin Cu(In,Ga)Se₂ solar cells. *Progr. Photovolt.* **22**, 1023–1029 (2014).
- 9 Dahan, N., Jehl, Z., Hildebrandt, T., Greffet, J.-J., Guillemoles, J.-F., Lincot, D. & Naghavi, N. Optical approaches to improve the photocurrent generation in Cu(In,Ga)Se₂ solar cells with absorber thicknesses down to 0.5 μm. *J. Appl. Phys.* **112**, 094902 (2012).
- 10 van Lare, C., Yin, G., Polman, A. & Schmid, M. Light coupling and trapping in ultrathin Cu(In,Ga)Se₂ solar cells using dielectric scattering patterns. *ACS Nano* **9**, 9603–9613 (2015).
- 11 Kurokawa, K., Kazmerski, L. L., McNelis, B., Yamaguchi, M., Wronski, C. & Sinke, W. C. (eds). in *Proc. 3rd World Conference Vol. 341 344–347* (Osaka, Japan, 2003).
- 12 Mutitu, J. G., Obahiagbon, U., Shi, S., Shafarman, W. & Prather, D. W. Light trapping in thin-film Cu(In,Ga)Se₂ solar cells. *IEEE J. Photovolt.* **4**, 948–953 (2014).
- 13 Freundlich, A. & Kurtz, S. (eds) in *Photovoltaic Specialist Conference (PVSC), 2015 IEEE 42nd 1–3* (New Orleans, USA, 2015).
- 14 Yin, G., Brackmann, V., Hoffmann, V. & Schmid, M. Enhanced performance of ultra-thin Cu(In,Ga)Se₂ solar cells deposited at low process temperature. *Sol. Energy Mater. Sol. Cells* **132**, 142–147 (2015).
- 15 Lundberg, O., Bodegård, M., Malmström, J. & Stolt, L. Influence of the Cu(In,Ga)Se₂ thickness and Ga grading on solar cell performance. *Progr. Photovolt.* **11**, 77–88 (2003).
- 16 Vermang, B., Fjällström, V., Gao, X. & Edoff, M. Improved rear surface passivation of Cu(In,Ga)Se₂ solar cells: a combination of an Al₂O₃ rear surface passivation layer and nanosized local rear point contacts. *IEEE J. Photovolt.* **4**, 486–492 (2014).
- 17 Scragg, J. J., Wätjen, J. T., Edoff, M., Ericson, T., Kubart, T. & Platzer-Björkman, C. A Detrimental reaction at the molybdenum back contact in Cu₂ZnSn(S,Se)₄ thin-film solar cells. *J. Am. Chem. Soc.* **134**, 19330–19333 (2012).
- 18 Redinger, A. & Siebentritt, S. Coevaporation of Cu₂ZnSnSe₄ thin films. *Appl. Phys. Lett.* **97**, 092111 (2010).
- 19 Bag, S., Gunawan, O., Gokmen, T., Zhu, Y., Todorov, T. K. & Mitzi, D. B. Low band gap liquid-processed CZTSe solar cell with 10.1% efficiency. *Energ Environ. Sci.* **5**, 7060–7065 (2012).
- 20 Shin, B., Gunawan, O., Zhu, Y., Bojarczuk, N. A., Chey, S. J. & Guha, S. Thin film solar cell with 8.4% power conversion efficiency using an earth-abundant Cu₂ZnSnS₄ absorber. *Progr. Photovolt.* **21**, 72–76 (2013).
- 21 Liu, F., Sun, K., Li, W., Yan, C., Cui, H., Jiang, L., Hao, X. & Green, M. A. Enhancing the Cu₂ZnSnS₄ solar cell efficiency by back contact modification: inserting a thin TiB₂ intermediate layer at Cu₂ZnSnS₄/Mo interface. *Appl. Phys. Lett.* **104**, 051105 (2014).
- 22 Watjen, J. T., Scragg, J. J., Edoff, M., Rubino, S. & Platzer-Björkman, C. Cu out-diffusion in kesterites—a transmission electron microscopy specimen preparation artifact. *Appl. Phys. Lett.* **102**, 051902–051904 (2013).
- 23 Zhou, F., Zeng, F., Liu, X., Liu, F., Song, N., Yan, C., Pu, A., Park, J., Sun, K. & Hao, X. Improvement of J_{sc} in a Cu₂ZnSnS₄ solar cell by using a thin carbon intermediate layer at the Cu₂ZnSnS₄/Mo interface. *ACS Appl. Mater. Inter.* **7**, 22868–22873 (2015).
- 24 Kumar, M., Dubey, A., Adhikari, N., Venkatesan, S. & Qiao, Q. Strategic review of secondary phases, defects and defect-complexes in kesterite CZTS-Se solar cells. *Energ Environ. Sci.* **8**, 3134–3159 (2015).
- 25 Zhu, X., Zhou, Z., Wang, Y., Zhang, L., Li, A. & Huang, F. Determining factor of MoSe₂ formation in Cu(In,Ga)Se₂ solar cells. *Sol. Energy Mater. Sol. Cells* **101**, 57–61 (2012).
- 26 Shin, B., Bojarczuk, N. A. & Guha, S. On the kinetics of MoSe₂ interfacial layer formation in chalcogen-based thin film solar cells with a molybdenum back contact. *Appl. Phys. Lett.* **102**, 091907–091904 (2013).
- 27 Altamura, G., Grenet, L., Roger, C., Roux, F., Reita, V., Fillon, R., Fournier, H., Perraud, S. & Mariette, H. Alternative back contacts in kesterite Cu₂ZnSn(S_{1-x}Se_x)₄ thin film solar cells. *J. Renew. Sustain. Energy* **6**, 011401 (2014).
- 28 Lopez-Marino, S., Placidi, M., Perez-Tomas, A., Llobet, J., Izquierdo-Roca, V., Fontane, X., Fairbrother, A., Espindola-Rodríguez, M., Sylla, D., Perez-Rodríguez, A. & Saucedo, E. Inhibiting the absorber/Mo-back contact decomposition reaction in Cu₂ZnSnSe₄ solar cells: the role of a ZnO intermediate nanolayer. *J. Mater. Chem. A* **1**, 8338–8343 (2013).
- 29 Li, W., Chen, J., Cui, H., Liu, F. & Hao, X. Inhibiting MoS₂ formation by introducing a ZnO intermediate layer for Cu₂ZnSnS₄ solar cells. *Mater. Lett.* **130**, 87–90 (2014).
- 30 Shin, B., Zhu, Y., Bojarczuk, N. A., Chey, S. J. & Guha, S. Control of an interfacial MoSe₂ layer in Cu₂ZnSnSe₄ thin film solar cells: 8.9% power conversion efficiency with a TiN diffusion barrier. *Appl. Phys. Lett.* **101**, 053903–053904 (2012).
- 31 Scragg, J. J., Kubart, T., Wätjen, J. T., Ericson, T., Linnarsson, M. K. & Platzer-Björkman, C. Effects of back contact instability on Cu₂ZnSnS₄ devices and processes. *Chem. Mater.* **25**, 3162–3171 (2013).
- 32 Cui, H., Liu, X., Liu, F., Hao, X., Song, N. & Yan, C. Boosting Cu₂ZnSnS₄ solar cell efficiency by a thin Ag intermediate layer between absorber and back contact. *Appl. Phys. Lett.* **104**, 041115 (2014).
- 33 Lee, Y. S., Gershon, T., Todorov, T. K., Wang, W., Winkler, M. T., Hopstaken, M., Gunawan, O. & Kim, J. Atomic layer deposited aluminum oxide for interface passivation of Cu₂ZnSn(S,Se)₄ thin-film solar cells. *Adv. Energy Mater.* **6**, 1600198 (2016).
- 34 Liu, F., Lai, Y., Liu, J., Wang, B., Kuang, S., Zhang, Z., Li, J. & Liu, Y. Characterization of chemical bath deposited CdS thin films at different deposition temperature. *J. Alloy Compd.* **493**, 305–308 (2010).
- 35 Liu, F., Yan, C., Huang, J., Sun, K., Zhou, F., Stride, J. A., Green, M. A. & Hao, X. Nanoscale microstructure and chemistry of Cu₂ZnSnS₄/CdS interface in kesterite Cu₂ZnSnS₄ solar cells. *Adv. Energy Mater.* **6**, 1600706 (2016).
- 36 Wei, L., Jian, C., Chang, Y., Fangyang, L. & Xiaojing, H. Transmission electron microscopy analysis for the process of crystallization of Cu₂ZnSnS₄ film from sputtered Zn/CuSn precursor. *Nanotechnology* **25**, 195701 (2014).
- 37 Vermang, B., Ren, Y., Donzel-Gargand, O., Frisk, C., Joel, J., Salomé, P., Borme, J., Sadewasser, S., Platzer-Björkman, C. & Edoff, M. Rear surface optimization of CZTS solar cells by use of a passivation layer with nanosized point openings. *IEEE J. Photovolt.* **6**, 332–336 (2016).
- 38 Hsu, W.-W., Chen, J. Y., Cheng, T.-H., Lu, S. C., Ho, W.-S., Chen, Y.-Y., Chien, Y.-J. & Liu, C. W. Surface passivation of Cu(In,Ga)Se₂ using atomic layer deposited Al₂O₃. *Appl. Phys. Lett.* **100**, 023508 (2012).
- 39 Hsu, W.-C., Repins, I., Beall, C., DeHart, C., Teeter, G., To, B., Yang, Y. & Noufi, R. The effect of Zn excess on kesterite solar cells. *Sol. Energy Mater. Sol. Cells* **113**, 160–164 (2013).
- 40 Ito, K. *Copper Zinc Tin Sulfide-Based Thin Film Solar Cells* (Wiley, New York, USA, 2015).
- 41 Sun, K., Liu, F., Yan, C., Zhou, F., Huang, J., Shen, Y., Liu, R. & Hao, X. Influence of sodium incorporation on kesterite Cu₂ZnSnS₄ solar cells fabricated on stainless steel substrates. *Sol. Energy Mater. Sol. Cells* **157**, 565–571 (2016).
- 42 Kumar, A., Banyai, D., Ahluwalia, P. K., Pandey, R. & Karna, S. P. Electronic stability and electron transport properties of atomic wires anchored on the MoS₂ monolayer. *Phys. Chem. Chem. Phys.* **16**, 20157–20163 (2014).
- 43 Yang, L. C. & Rockett, A. Cu–Mo contacts to CuInSe₂ for improved adhesion in photovoltaic devices. *J. Appl. Phys.* **75**, 1185–1189 (1994).
- 44 Ohnesorge, B., Weigand, R., Bacher, G., Forchel, A., Riedl, W. & Karg, F. H. Minority-carrier lifetime and efficiency of Cu(In,Ga)Se₂ solar cells. *Appl. Phys. Lett.* **73**, 1224–1226 (1998).
- 45 Young, M. J., Musgrave, C. B. & George, S. M. Growth and characterization of Al₂O₃ atomic layer deposition films on sp²-graphitic carbon substrates using NO₂/trimethylaluminum pretreatment. *ACS Appl. Mater. Inter.* **7**, 12030–12037 (2015).
- 46 Sites, J. R. & Mauk, P. H. Diode quality factor determination for thin-film solar cells. *Sol. Cells* **27**, 411–417 (1989).



This work is licensed under a Creative Commons Attribution 4.0 International License. The images or other third party material in this article are included in the article's Creative Commons license, unless indicated otherwise in the credit line; if the material is not included under the Creative Commons license, users will need to obtain permission from the license holder to reproduce the material. To view a copy of this license, visit <http://creativecommons.org/licenses/by/4.0/>

© The Author(s) 2017

Supplementary Information accompanies the paper on the NPG Asia Materials website (<http://www.nature.com/am>)